

Finite element simulation of bone remodelling in the human mandible surrounding dental implant

Dr Zhiqiang Lian¹

Telephone: +86 (0)411 84708408, Fax: +86 (0)411 84708769, Email: lianqz75@dlut.edu.cn

Associate Professor Hong Guan²

Telephone: +61 (0)7 5552 8708, Fax: +61 (0)7 5552 8065, Email: h.guan@griffith.edu.au

Professor Saso Ivanovski³, Listerine Chair Professor of Periodontology

Telephone: +61 (0)7 5678 0741, Fax: +61 (0)7 5678 0708,

Email: s.ivanovski@griffith.edu.au

Professor Yew-Chaye Loo², Foundation Chair of Civil Engineering,

Director, Internationalisation and Professional Liaison,

Science, Environment, Engineering and Technology Group

Telephone: +61 (0)7 5552 8105, Fax: +61 (0)7 5552 8065, Email: y.loo@griffith.edu.au

Professor Newell Johnson³, Professor of Dental Research and Foundation Chair

Telephone: +61 (0)7 5678 0713, Fax: +61 (0)7 5678 0708, Email: n.johnson@griffith.edu.au

Professor Hongwu Zhang¹

Telephone: +86 (0)411 84708408, Fax: +86 (0)411 84708769, Email: zhanghw@dlut.edu.cn

¹State Key Laboratory of Structural Analysis for Industrial Equipment, Department of Engineering Mechanics, Dalian University of Technology, Dalian, 116023, China.

²Griffith School of Engineering, Griffith University Gold Coast Campus, Queensland 4222, Australia.

³Griffith Health Institute, Griffith University Gold Coast Campus, Queensland 4222, Australia.

Address correspondence to Zhiqiang Lian, State Key Laboratory of Structural Analysis for Industrial Equipment, Department of Engineering Mechanics, Dalian University of Technology, Dalian, 116023, China

Finite element simulation of bone remodelling in the human mandible surrounding dental implant

Z.Q. Lian¹, H. Guan², S. Ivanovski³, Y.C. Loo², N. Johnson³, H.W. Zhang¹

¹*State Key Laboratory of Structural Analysis for Industrial Equipment, Department of Engineering Mechanics, Dalian University of Technology, Dalian, 116023, China.*

²*Griffith School of Engineering, Griffith University Gold Coast Campus, Queensland 4222, Australia.*

³*School of Dentistry and Oral Health, Griffith University Gold Coast Campus, Queensland 4222, Australia.*

Abstract

Dental implant is a biocompatible titanium device surgically placed into the jaw bone to support a prosthetic tooth crown in order to replace missing teeth. However, placement of an implant changes the normal mechanical environment of jawbone, which causes the bone density to redistribute and adapt to the new environment by remodelling. This study aims to predict the density distribution in human jawbone surrounding a dental implant. Based on some popular, yet distinctive theories for bone remodelling, a new algorithm is proposed which takes into account both the ‘lazy zone’ effect and the self-organisational control process. The proposed algorithm is firstly verified by a two-dimensional (2D) plate model simulating bone tissue, then, a 2D finite element model of implant and jawbone is studied. The effects of two parameters, viz the reference value of strain energy density (SED) and the ‘lazy zone’ region, on density distribution are also investigated. The proposed algorithm is proven to be effective and the predicted density distribution patterns correlate well with clinical observations. This study has demonstrated that consideration of the lazy zone is less important than consideration of the stress and strain (quantified as SED) induced within the bone.

Keywords: bone remodelling, density distribution, implant-bone system, finite element technique

1 Introduction

Dental implants provide the most efficient and economic long-term solution for replacing lost teeth [1]. However, according to the clinical investigation of Turkyilmaz and McGlumphy [2], placement of an implant changes the normal mechanical environment of jawbone, which causes bone density to redistribute and adapt to the new environment by remodelling. Implant bone restorations have become a clinically and scientifically accepted treatment modality over the past 20 years. The realization that implants made of commercially pure titanium attain direct bone to implant contact initiated this revolution in oral rehabilitation. This phenomenon of osseointegration (or functional ankylosis) was first described by Branemark et al. [3] and Schroeder et al. [4].

The direct union between the dental implant and bone, which is characteristic of osseointegration, means that occlusal forces during chewing function are transmitted to bone. Bone, as a living tissue, undergoes continuous adaptation and self-repair by resorption and formation, and is capable of optimizing its internal structure under the influence of external loads. The self-adaptation process, termed as ‘remodelling’, has an enormous effect on the overall behavior of the entire bone tissue throughout an individual’s lifetime. Following the early publication of Wolff [5], many theories describing the bone-adaptation process have been proposed. Carter [6] suggested that bone is ‘lazy’ in terms of poor reaction to mechanical signals, and there was recognition of the existence of a ‘lazy zone’ representing the range of stimulus within which no remodelling occurs.

The concept of 'lazy zone', recognising that a threshold stimulus needed to be exceeded for bone adaptation to occur, was incorporated by Huiskes et al. [7] who used the term strain energy density (SED) to describe the stresses and strains that control bone remodelling through bone formation and resorption. This theory has been developed further by Weinans et al. [8] and Turner et al. [9]. Mullender et al. [10] and Mullender and Huiskes [11] suggested a physiological approach to simulate bone remodelling which assumed that osteocytes are sensitive to mechanical loading and are active in controlling bone adaptation.

Computational simulation of bone remodelling generally involves finite element analysis for calculating stresses, strains and SEDs within the bone thereby determining how bone adapts itself in response to mechanical stimuli. The finite element method (FEM) was initially introduced to orthopedic biomechanics by Brekelmans et al. [12] and Rybicki et al. [13] to evaluate the stresses in human bone. Since then, the method has been successfully applied for stress analyses of bone and bone-related tissue. The above-mentioned theories of bone remodelling have been used successfully in conjunction with the FEM to predict density distribution in proximal femur [10,11,14] and bone adaptation following hip prosthetic implantation [7,15-18]. While these theories were essentially developed for orthopedics, they are generally applicable to jawbone surrounding a dental implant [19]. However, work in this area is limited. Mellal et al. [20] used three different stimuli (equivalent strain, equivalent stress and SED) to predict bone remodelling around a dental implant based on the existing theories and the results were compared with in vivo data. Li et al. [21] developed a new bone remodelling algorithm by introducing an additional quadratic term based on the theory of Weinans et al. [8], which can simulate both underload and overload resorption. The algorithm was applied in conjunction with the FEM to a practical case of dental implant treatment. Under steady conditions, no overall changes in bone would be observable due to the balance in resorption and formation. However when the implant is placed into mandible, the mechanical environment of jawbone changes accordingly, hence the balance of bone resorption and formation is no longer maintained. From a clinical viewpoint, better understanding of the way that functional forces can affect the remodelling of bone is important in terms of identifying minimum and maximum loading forces required for the maintenance of stable osseointegration during function, as well as preventing overload that can lead to implant failure.

In this paper, a new algorithm for bone remodelling is proposed based on the existing theories of Huiskes et al. [7], Weinans et al. [8], Mullender et al. [10] and Mullender and Huiskes [11]. The proposed algorithm is verified by a 2D plate model simulating bone tissue studied previously by Weinans et al. [8] and Mullender et al. [10], which confirms its accuracy and reliability. To demonstrate the ability of the proposed algorithm in predicting density distribution of bone surrounding a dental implant, a 2D finite element model of implant and jawbone is studied. The effects of two parameters viz the reference value of SED and 'lazy zone' region, on density distribution are also investigated and discussed in some detail.

2 The Existing Bone Remodelling Theory

Jawbone surrounding a dental implant experiences stress and strain when the implant is loaded. Bone biomechanically reacts by altering its apparent density. Among a number of bone remodelling theories [7-11,14,15,22-25], two popular yet

distinctive ones are summarized in the following subsections followed by the presentation of the proposed algorithm.

2.1 Huiskes and Weinans Theory

A popular bone remodelling theory suggested by Huiskes et al. [7] and Weinans et al. [8] states that:

$$\frac{d\rho}{dt} = \begin{cases} B\left(\frac{U}{\rho} - (1+s)K\right) & \text{if } \frac{U}{\rho} > (1+s)K \\ 0 & \text{if } (1-s)K \leq \frac{U}{\rho} \leq (1+s)K \\ B\left(\frac{U}{\rho} - (1-s)K\right) & \text{if } \frac{U}{\rho} < (1-s)K \end{cases} \quad (1)$$

where $d\rho/dt$ is the rate of change in density; ρ is the apparent density of bone tissue; B is a constant regulating the rate of the remodelling process; s is in percentage denoting the region of the ‘lazy zone’ around the threshold value K , which is a reference value for SED (Fig. 1); the ‘lazy zone’ describes the bone not having a net change in apparent density, and is defined as U/ρ ; U is the SED which can be expressed as:

$$U = \frac{1}{2} \boldsymbol{\sigma} \cdot \boldsymbol{\varepsilon} \quad (2)$$

where $\boldsymbol{\sigma}$ and $\boldsymbol{\varepsilon}$ are respectively the stress and strain tensors of the bone tissue.

For multiple-load cases, the SED can be expressed as:

$$U = \frac{1}{n} \sum_{i=1}^n U_i \quad (3)$$

where n is the number of load cases and U_i is the SED under load case i .

‘[Insert Figure 1 about here]’

This algorithm was applied to predict density distribution in normal proximal femur with results showing a discontinuous pattern [8]. As discussed by Ruimerman and Huiskes [26], only when the density distributions were locally averaged from discontinuous density patterns in the femoral head where the trabecular bone is located, the resulting density distributions correlate well with those in a real proximal femur. This algorithm showed an unstable condition in its mathematical operation. Due to the nature of differential equations used in the algorithm to describe the adaptive remodelling process, the simulation produces discontinuous configurations, a phenomenon called ‘checker-board’.

2.2 Mullender et al. and Mullender and Huiskes Theory

Not having intrinsically different biological nature from the theory of Huiskes et al. [7] and Weinans et al. [8], Mullender et al. [10] and Mullender and Huiskes [11] suggested a new algorithm which simulated bone remodelling as a self-organisational control process. In their theory, bone is assumed to have N sensor cells distributed uniformly over its volume. An arbitrary sensor i measures a signal S_i , which is given as:

$$S_i = \frac{U_i}{\rho_i} \quad (4)$$

where ρ_i is the density at the location of the sensor. The density $\rho(\mathbf{x},t)$ at location \mathbf{x} is regulated by the stimulus value $\Phi(\mathbf{x},t)$, to which all sensor cells contribute, relative to their distance from \mathbf{x} . Hence,

$$\Phi(\mathbf{x},t) = \sum_{i=1}^N f_i(\mathbf{x})(S_i - K) \quad (5)$$

where N is the total number of sensors. In the finite element simulation, N is equal to the total number of elements; $f_i(\mathbf{x})$ is a spatial influence function given as:

$$f_i(\mathbf{x}) = e^{-[d_i(\mathbf{x})/D]} \quad (6)$$

where $d_i(\mathbf{x})$ is the distance between sensor i and location \mathbf{x} , D is the rate of the spatial influence reduction. Note that D represents the distance from a sensor at which location its effect is reduced to e^{-1} , i.e. 36.8%.

The density $\rho(\mathbf{x},t)$ is now governed by the rate:

$$\frac{d\rho(\mathbf{x},t)}{dt} = \tau\Phi(\mathbf{x},t), \text{ with } 0 < \rho(\mathbf{x}) \leq \rho_{max} \quad (7)$$

where ρ_{max} is the maximum density of cortical bone, τ is a time constant regulating the rate of the process, and t is the remodelling time. It should be noted that t is a unitless quantity and does not represent real clinical time.

This algorithm was used to predict density distribution for a 2D plate model previously studied by Mullender et al. [10]. The model produced trabecular-like structures without the ‘checker-board’ patterns. This is presented later in Section 4. It should be noted that the checker-board effect produced by the phenomenological models like the one of Weinans et al. [8] has been completely solved by different techniques including extrapolation to the nodes [25] or using non-local stimuli [10,11]. The checker-board phenomenon is believed to be attributable to the softening induced by resorption rather than remodelling itself. When using the non-local definition of the stimulus as a sum of the signal of different osteocytes near the point under concerned, Mullender et al.'s model [10, 11] does not produce ‘checker-board’ patterns.

3 The Proposed Algorithm

The existing two theories have both shown to exhibit advantages and disadvantages. Huiskes and Weinans’s theory takes into account the ‘lazy zone’ effect but it is unstable in its mathematical operation leading to a discontinuous and an inevitable ‘checker-board’ pattern. Mullender’s theory, on the other hand, is physiologically and mechanically more consistent and ‘checker-board’ phenomena can be effectively eliminated. However the effect of ‘lazy zone’ was not considered in Mullender’s theory. The ‘lazy zone’ effect, initially proposed by Carter [6] based on experimental investigation, has been verified by Rubin and Lanyon [27] to be an important factor which should be considered in the simulation of the remodelling process.

To overcome the shortcomings of the above two theories, a new algorithm combining these two theories is proposed herein. Based on Mullender’s work, the following governing equation is proposed, taking into account the ‘lazy zone’ effect. For an arbitrary sensor i ,

$$\frac{d\rho_i(\mathbf{x},t)}{dt} = \tau\Phi_i(\mathbf{x},t) \quad (8)$$

and

$$\Phi_i(\mathbf{x},t) = \begin{cases} \sum_{i=1}^N f_i(\mathbf{x}) \left(\frac{U_i}{\rho_i} - (1+s)K \right) & \text{if } \frac{U_i}{\rho_i} > (1+s)K \\ 0 & \text{if } (1-s)K \leq \frac{U_i}{\rho_i} \leq (1+s)K, \text{ with } 0 < \rho_i(\mathbf{x}) \leq \rho_{max} \\ \sum_{i=1}^N f_i(\mathbf{x}) \left(\frac{U_i}{\rho_i} - (1-s)K \right) & \text{if } \frac{U_i}{\rho_i} < (1-s)K \end{cases} \quad (9)$$

where $f_i(\mathbf{x})$ is the spatial influence function in the same form as in Eq. (6).

In the finite element simulation, it is assumed that each element contains one sensor which is located at the centre of the element. As the apparent density of bone tissue changes during the process of remodelling, Young's modulus changes accordingly. Some empirical relationships between apparent density and mechanical properties of bone have been established experimentally [28-31]. In the present study, Young's modulus E at location \mathbf{x} is calculated according to Currey [29] and Rice et al. [31] as

$$E(\mathbf{x},t) = C\rho(\mathbf{x},t)^\gamma \quad (10)$$

where ρ is the apparent density of bone tissue; C and γ are constants.

In the iterative finite element analysis process, the governing equation (8) is necessary to be rewritten as:

$$\rho_i(t + \Delta t) = \rho_i(t) + \Delta t \tau \Phi_i(t) \quad (11)$$

where Δt is the time step in the iteration process; $\Phi(t)$ is in the same form as in Eq. (9). Iteration is continued until no more significant changes occur in the resulting density distribution.

4 Results

The proposed algorithm is verified against a 2D plate model (see Fig. 2), studied by Weinans et al. [8] and Mullender et al. [10] to simulate density distribution within a bone tissue. The plate is loaded by a compressive stress over the top edge. A uniform initial density distribution of $\rho=0.8\text{g/cm}^3$ is taken. The bone tissue is assumed to be isotropic. The reference signal value $K=0.25\text{J/g}$, the maximum density $\rho_{max}=1.74\text{g/cm}^3$ and $\tau=1(\text{g/cm}^3)^2/(\text{MPa time-unit})$. To avoid numerical singularity, a minimum density $\rho_{min}=0.01\text{g/cm}^3$ is adopted instead of the lower bound set in Eq. (7). The plate is discretized into 40×40 four-node plane strain elements by using Strand7 Finite Element System (Strand7 Pty Ltd, Sydney, Australia). The influence parameter $D=0.025\text{mm}$, $C=100\text{MPa}/(\text{g/cm}^3)^2$ and $\gamma=2.0$, are the same as those adopted by Weinans et al. [8] and Mullender et al. [10]. For the purpose of comparison, the value s is initially set to zero meaning that the effect of 'lazy zone' is not considered in the analysis.

'[Insert Figure 2 about here]'

Fig. 3 compares the density distribution outcomes due to Mullender et al.'s [10] theory and the proposed algorithm. The predicted result shown in Fig. 3b bears a

strong resemblance to that of Mullender et al. (Fig. 3a), confirming the accuracy of the proposed algorithm. To evaluate the effect of ‘lazy zone’, a further analysis is carried out by setting $s=0.1$ while other parameters remain unchanged. When the ‘lazy zone’ effect is considered (Fig. 3c, $s=0.1$), the pattern of density distribution becomes smoother in shape as compared to that of $s=0$ (Fig. 3b), although the morphology is almost the same. The total area of grey regions (representing cancellous bone) is larger in Fig. 3c than in Fig. 3b suggesting that less bone adaptation (viz resorption and formation) occurs if the ‘lazy zone’ effect is considered.

‘[Insert Figure 3 about here]’

The predicted density distributions for the plate model agree well with the Mullender’s results, confirming the reliability of the proposed algorithm when taking into account both the ‘lazy zone’ effect and mathematical stability. The proposed algorithm is hence applied to simulate density distribution within a mandibular bone surrounding a dental implant.

A 2D representation of the implant and mandible is studied herein and the modelling scheme follows that of a previous study [32]. It should be noted that this is a preliminary study dealing with a new remodelling algorithm aimed at combining the advantages of the abovementioned two existing methodologies. For the purpose of initial verification, 2D analysis is undertaken to obtain fundamental understanding of the remodelling process. 3D analysis will be conducted in the future so that detailed implant geometry can be considered and more accurate solutions be obtained.

The different types of bone, i.e. cortical and cancellous bone are identified in the model based on CT images which were obtained from Mimics (Materialise NV, Belgium). The implant dimensions are based on those of Neoss (Neoss Limited, UK). Fig. 4a shows the dimensions of the entire implant and jawbone model. The implant is conical with 2 degrees of taperage and has a helical thread. In this particular finite element model, the total numbers of plane strain elements are respectively 1100 for the crown, 220 for the abutment, 469 for the abutment screw, 2030 for the implant, 2704 for the cortical bone, and 6750 for the cancellous bone. The load and boundary conditions shown in Fig. 4b are based on the work of Chou et al. [33] in which the implant system is loaded with an occlusal load of 100N on the crown at an angle of 11° and a uniformly distributed pressure of 500kPa on the outer periphery of the cortical bone, representing forces due to jaw flexure [33].

‘[Insert Figure 4 about here]’

An extensive literature review by van Staden et al. [34] indicates that the assumed range of Young’s modulus for cortical bone varies from 5.57 to 22.8GPa and that of cancellous bone varies from 0.08 to 7.93GPa. Typical values of Young’s modulus (E) of bone and implant for the analysis are selected based on the work of Papavasiliou et al. [35], which are also detailed in Fig. 4b. The Poisson’s ratio for all components is taken as 0.3. The bone tissue and implant are assumed to be isotropic materials. Note that in this study a perfect connection between the implant and jawbone is assumed.

The remodelling is considered for cancellous bone only assuming a constant Young’s modulus of cortical bone (13.7GPa). A uniform initial density distribution

of $\rho=1.4\text{g/cm}^3$ is also assumed which corresponds to $E=7.93\text{GPa}$. In this case, a specific relationship between E and density ρ is chosen based on Carter and Hayes' study [28], i.e.:

$$E(\mathbf{x},t) = 3790 \times \rho^3 \quad (12)$$

where \mathbf{x} is the location of sensors; t is the remodelling time. The maximum and minimum densities are $\rho_{max}=1.5347\text{g/cm}^3$ and $\rho_{min}=0.064\text{g/cm}^3$ respectively which corresponds to Young's modulus of 13.7GPa and 1kPa . The 'lazy zone' effect s in Eq. (9) is taken as 0.1, the constant $\tau=1(\text{g/cm}^3)^2/(\text{MPa time-unit})$. The influence parameter $D=0.25$ mm.

To evaluate the 'lazy zone' effect on density distribution, different values of s are considered with a constant SED value $K=0.0052\text{J/g}$. The predicted results are shown in Fig. 5. When parameter s increases, the region of 'lazy zone' expands accordingly - hence more bone tissue remains 'lazy', i.e. neither resorption nor formation. This corresponds to a larger grey region on the lingual side of the implant (Fig. 5d). Although more 'lazy zone' is evident when s increases, the overall morphology does not vary significantly.

'[Insert Figure 5 about here]'

Different reference values K in Eq. (9) are also considered to evaluate the effects of threshold value of SED on the density distribution outcomes. The results shown in Fig. 6 indicate that when K increases, more bone tissue is resorbed in the surrounding jawbone, especially on the lingual side of the implant due to the oblique loading condition.

'[Insert Figure 6 about here]'

Fig. 7 shows the relationship between bone mass (for cancellous bone only) and two parameters s and K . When s increases by 300%, the weight w only increases by 2.08% correspondingly; when K increases by 16.7%, the weight w decreases by 4.5%. It can be deduced that bone mass increases slightly with an increase in the 'lazy zone' effect s (Fig. 7a) and decreases more noticeably with an increase in the reference value K (Fig. 7b). The results suggest that the parameter K has more significant effect than s on bone remodelling.

'[Insert Figure 7 about here]'

5 Discussion

This paper proposes a new algorithm for the study of bone remodelling around dental implants, which is a combination and further development of two existing and widely accepted bone remodelling theories. The algorithm takes into account both the 'lazy zone' effect and the self-organisational control process. It is shown to be accurate and reliable upon verification with a plate model simulating bone tissue. The algorithm is then used to predict density distribution in human jawbone surrounding a dental implant. The influence of two parameters viz the reference SED value K and the 'lazy zone' effect s on density distribution is also evaluated. The results indicate that K has more significant influence than s .

With an increasing value of K , a reduction in bone formation and an increase in

bone resorption are evident, and *vice versa*. There is no general rule or criterion in published literature on the selection of the reference value K . It is found in this study that a median value among all the SEDs is appropriate to yield a satisfactory density distribution outcome.

Fig. 8 compares the predicted density distribution in cancellous bone surrounding a dental implant with a published clinical observation by Watzak et al. [36] and a numerical prediction by Chou et al. [33]. Fig. 8a shows Watzak's clinical observation of density distribution on baboons and Fig. 8b presents Chou et al.'s bone remodelling prediction around a dental implant. The predicted result (with $K=0.0052$ J/g) due to the proposed algorithm is re-produced in Fig. 8c. The overall density distributions are found to be quite similar for three cases in terms of the trabecular-like pattern and the blank area below the implant. This is particularly true when comparing Fig. 8b and Fig. 8c. Lin et al.'s computational prediction indicated that the average density of peri-implant cancellous bone increases throughout the remodelling period [37], which is consistent with our results. However, due to the simplification of the finite element model, discrepancies in density distribution do exist between the present computational modelling outcome and the clinical observation.

‘[Insert Figure 8 about here]’

As far as the implant/bone connection is concerned, Roberts [38] found that even ‘clinically successful’ implants had less than half of the intraosseous interface in direct contact with bone. Block et al. [39] found similar levels of osseointegration for loaded implants in dogs. In this study, a perfect connection between the implant and jawbone is assumed due to the difficulties in accessing accurate clinical data on contact percentage. The simplification of the interface may have some influence on the resulting density distribution which should be investigated further.

It should also be noted that this study is a preliminary attempt in developing a new bone remodelling algorithm suitable for computer simulation of the highly complex processes of bone healing and remodelling. In addition to the assumed perfect implant/bone connection, this study also employs a simplified and fixed loading condition. This is considerably different from the actual masticatory forces which always vary in both magnitude and direction. Hence, a discrepancy between the resulting density distribution (Fig. 6) and the true anatomy of jawbone is expected. Further work should be done to evaluate the effects of other parameters which may also affect density distribution within the jawbone surrounding a dental implant. Furthermore, the approximation and simplification made in this study should be examined in future research, in particular in regard to the influence of different percentages of osseointegration on bone remodelling associated with dental implants.

6 Conclusions

Whilst further optimization of the algorithm described here is desirable, our model has been shown to correlate well with clinical observations. An important consideration is that the ‘lazy zone’, representing the range of stimuli where no bone remodelling occurs around a dental implant, is less important than consideration of the ‘strain energy density’ representing the stresses and strains induced within the bone. Improved understanding of the factors which influence bone remodelling around osseointegrated dental implants is important in

quantifying the forces compatible with maintaining successful osseointegration and preventing overload leading to implant failure. To this end, the newly developed algorithm incorporating elements from previous theories more closely replicates the clinical situation.

Acknowledgements

The financial support from the 2006 Griffith University Research Grant scheme and the assistance Dr. Rudi van Staden are gratefully acknowledged.

References

1. Bouchard, P., Renouard, F., Bourgeois, D., Fromentin, O., Jeanneret, M.H., Beresniak, A.: Cost-effectiveness modeling of dental implant vs. bridge. *Clin. Oral Implants Res.* **20**, 583-587 (2009)
2. Turkyilmaz, I., McGlumphy, E.A.: Influence of bone density on implant stability parameters and implant success: a retrospective clinical study. *BMC Oral Health.* **8**:32 (2008)
3. Brånemark, P.I., Hansson, B.O., Adell, R., Breine, U., Lindström, J., Hallén, O., Ohman, A.: Osseointegrated implants in the treatment of the edentulous jaw. Experience from a 10-year period. *Scand. J. Plast. Reconst. Surg. Suppl.* **7**, 1-132 (1977)
4. Schroeder, A., van der Zypen, E., Stich, H., Sutter, F.: The reactions of bone, connective tissue, and epithelium to endosteal implants with titanium-sprayed surfaces. *J. Maxillofacial Surgery.* **9**, 15-25 (1981)
5. Wolff, J.L.: The law of bone remodelling. Translated by Maquet P, Furlong R, in 1986.: Springer-Verlag, Berlin (1892)
6. Carter, D.R.: Mechanical loading histories and cortical bone remodeling. *Calcif. Tissue Int.* **36**, 19-24 (1984)
7. Huiskes, R., Weinans, H., Grootenboer, H.J., Dalstra, M., Fudala, B., Slooff, T.J.: Adaptive bone-remodeling theory applied to prosthetic design analysis. *J. Biomech.* **20**, 1135-1150 (1987)
8. Weinans, H., Huiskes, R., Grootenboer, H.J.: The behavior of adaptive bone-remodeling simulation models. *J. Biomech.* **25**, 1425-1441 (1992)
9. Turner, C.H., Anne, V., Pidaparti, R.M.V.: A uniform strain criterion for trabecular bone adaptation, do continuum-level strain gradients drive adaptation. *J. Biomech.* **30**, 555-563 (1997)
10. Mullender, M.G., Huiskes, R., Weinans, H.: A physiological approach to simulation of bone remodelling as a self-organizational control process. *J. Biomech.* **27**, 1389-1394 (1994)
11. Mullender, M.G, Huiskes, R.: Proposal for the regulatory mechanism of Wolff's law. *J. Orthop. Res.* **13**, 503-512 (1995)
12. Brekelmans, W.A.M., Poort, H.W., Slooff, T.J.J.H.: A new method to analyse the mechanical behavior of skeletal parts. *Acta Orthop. Scand.* **43**, 301-317 (1972)
13. Rybicki, E.F., Simonen, F.A., Weis, E.B.: On the mathematical analysis of stress in human femur. *J. Biomech.* **5**, 203-215 (1972)
14. Carter, D.R., Orr, T.E., Fyhrie, D.P.: Relationships between loading history and femoral cancellous bone architecture. *J. Biomech.* **22**, 231-244 (1989)
15. Huiskes, R., Weinans, H., van Rietbergen, B.: The relationship between stress shielding and bone resorption around total hip stems and the effects of flexible materials. *Clin. Orthop. Relat. Res.* **274**, 124-134 (1992)
16. Kerner, J., Huiskes, R., van Lenthe, G.H., Weinans, H., van Rietbergen, B., Engh, C.A., Amis, A.A.: Correlation between pre-operative periprosthetic bone density and post-operative bone loss in THA can be explained by strain-adaptive remodelling. *J. Biomech.* **32**, 695-703 (1999)
17. van Rietbergen, B., Huiskes, R., Weinans, H., Sumner, D.R., Turner, T.M., Galante, J.O.: ESB Research Award 1992. The mechanism of bone remodelling and resorption around press-fitted THA stems. *J. Biomech.* **26**, 369-382 (1993)
18. Weinans, H., Huiskes, R., van Rietbergen, B., Sumner, D.R., Turner, T.M., Galante, J.O.: Adaptive bone remodelling around bonded noncemented total hip arthroplasty, a comparison between animal experiments and computer simulation. *J. Orthop. Res.* **11**, 500-513 (1993)
19. Duyck, J., Ronold, H.J., Van Oosterwyck, H., Naert, I., Sloten, J.V., Ellingsen, J.E.: The influence of static and dynamic loading on marginal bone reactions around osseointegrated implants: an animal experimental study. *Clin. Oral Implants Res.* **12**, 207-218 (2001)
20. Mellal, A., Wiskott, H.W.A., Scherrer, S.S., Belser, U.C.: Stimulating effect of implant loading on surrounding bone. Comparison of three numerical models and validation by in vivo data. *Clin.*

Oral Implants Res. **15**, 239-248 (2004)

21. Li, J., Li, H., Shi, L., Fok, A.S.L., Ucer, C., Devlin, H., Houner, H., Silikas, N.: A mathematical model for simulating the bone remodelling process under mechanical stimulus. *Dent. Mater.* **23**, 1073-1078 (2007)
22. Carter, D.R., Fyhrie, D.P., Whalen, R.T.: Trabecular bone density and loading history: regulation of connective tissue biology by mechanical energy. *J. Biomech.* **20**, 785-794 (1987)
23. Hart, R.T., Davy, D.T.: Theories of bone modelling and remodelling. 1st ed. Cowin, S.C. *Bone Mechanics*, CRC Press, Boca Raton (1989)
24. Fyhrie, D.P., Carter, D.R.: Femoral head apparent density distribution predicted from bone stresses. *J. Biomech.* **23**, 1-10 (1990)
25. Jacobs, C.R., Simo, J.C., Bearpre, G.S., Carter, D. R.: Adaptive bone remodeling incorporating simultaneous density and anisotropy considerations. *J. Biomech.* **30**, 603-613 (1997)
26. Ruimerman, R., Huiskes, R.: Development of a unifying theory for mechanical adaptation and maintenance of trabecular bone. *Theor. Issues in Ergon. Sci.* **6**, 225-238 (2005)
27. Rubin, C.T., Lanyon, L.E.: Regulation of bone mass by mechanical strain magnitude. *Calcif. Tissue Int.* **37**, 411-417 (1985)
28. Carter, D.R., Hayes, W.C.: The compressive behavior of bone as a two-phase porous structure. *J. Bone Joint Surg. [Am]* **59**, 954-962 (1977)
29. Currey, J.D.: The effect of porosity and mineral content on the Young's modulus of elasticity of compact bone. *J. Biomech.* **21**, 131-139 (1988)
30. Morgan, E.F., Bayraktar, H.H., Keaveny, T.M.: Trabecular bone modulus-density relationships depend on anatomic site. *J. Biomech.* **36**, 897-904 (2003)
31. Rice, J.C., Cowin, S.C., Bowman, J.A.: On the dependence of the elasticity and strength of cancellous bone on apparent density. *J. Biomech.* **21**, 155-168 (1988)
32. Guan, H., van Staden, R., Loo, Y.C., Johnson, N.W., Ivanovski, S., Meredith, N.: Influence of bone and dental implant parameters on stress distribution in mandible - A finite element study. *Int. J. Oral Maxillofac. Implants* **24**, 866-876 (2009)
33. Chou, H.Y., Jagodnik, J.J., Muftu, S.: Predictions of bone remodeling around dental implant systems. *J. Biomech.* **41**, 1365-1373 (2008)
34. van Staden, R.C., Guan, H., Loo, Y.C.: Application of the finite element method in dental implant research. *Comput. Methods Biomech. Biomed. Engin.* **9**, 257-270 (2006)
35. Papavasiliou, G., Kamposiora, P., Bayne, S.C., Felton, D.A.: 3D-FEA of osseointegration percentages and patterns on implant-bone interfacial stresses. *J. Dent.* **25**, 485-491 (1997)
36. Watzak, G., Zechner, W., Ulm, C., Tangl, S., Tepper, G., Watzek, G.: Histologic and histomorphometric analysis of three types of dental implants following 18 months of occlusal loading: a preliminary study in baboons. *Clin. Oral Implants Res.* **16**, 408-416 (2005)
37. Lin, D., Li, Q., Li, W., Duckmanton, N., Swain, M.: Mandibular bone remodelling induced by dental implant. *J. Biomech.* **43**, 287-293 (2010)
38. Roberts, W.E.: Bone tissue interface. *J. Dent. Educ.* **52**, 804-809 (1988)
39. Block, M.S., Finger, I.M., Fontenot, M.G., Kent, J.N.: Loaded hydroxylapatite-coated and grit-blasted titanium implants in dogs. *Int. J. Oral Maxillofac. Implants* **4**, 219-225 (1989)

Figure Legends

- Figure 1. The assumed local adaptation as a function of the SED with the effect of 'lazy zone'
- Figure 2. 2D plate model simulating bone tissue (Carter and Hayes[28], Weinans et al.[8])
- Figure 3. Comparison of density distribution: **a** Mullender et al.'s[10] prediction with $s=0$; **b** predicted result with $s=0$; and **c** predicted result with $s=0.1$
- Figure 4. Finite element model of implant and jawbone: **a** dimensions; and **b** load, boundary conditions and material properties
- Figure 5. Influence of 'lazy zone' effect on the density distribution of jawbone surrounding dental implant: **a** $s=0.1$; **b** $s=0.2$; **c** $s=0.3$; and **d** $s=0.4$
- Figure 6. Influence of reference SED value K on the density distribution of jawbone surrounding dental implant: **a** $K=0.0048$ J/g; **b** $K=0.005$ J/g; **c** $K=0.0052$ J/g; **d** $K=0.0054$ J/g; and **e** $K=0.0056$ J/g
- Figure 7. Influence of two parameters on bone mass: **a** 'lazy zone' effect s ; and **b** reference value K
- Figure 8. Comparison of predicted result with clinical observations: **a** density distribution on baboons; **b** Chou et al.'s [33] prediction; and **c** predicted result with $K=0.0052$ J/g

Figures

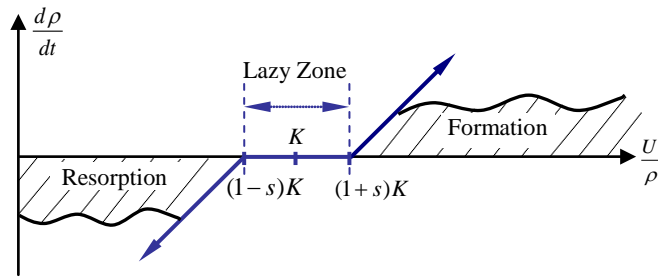


Fig. 1 The assumed local adaptation as a function of the SED with the effect of 'lazy zone'

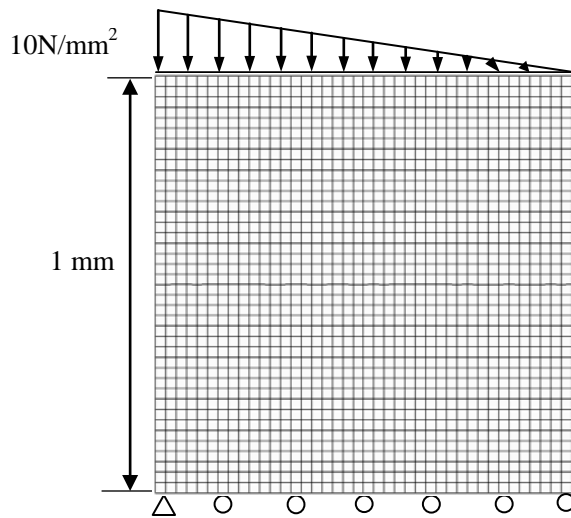


Fig. 2 2D plate model simulating bone tissue (Carter and Hayes [28], Weinans et al. [8])

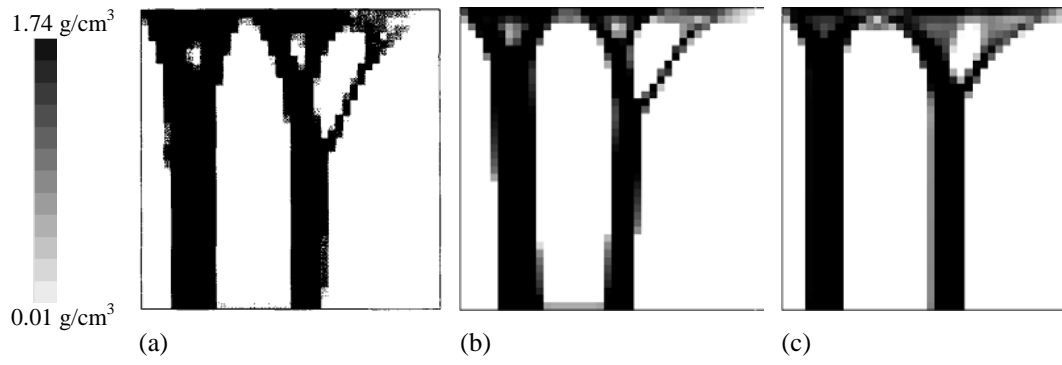


Fig. 3 Comparison of density distribution: **a** Mullender et al.'s [10] prediction with $s=0$; **b** predicted result with $s=0$; and **c** predicted result with $s=0.1$

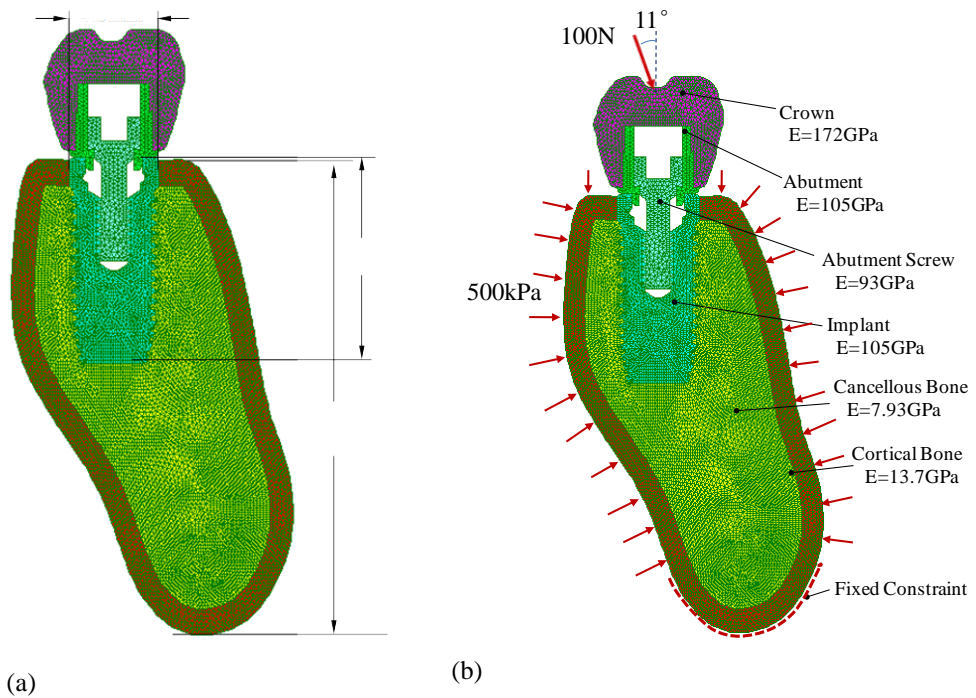


Fig. 4 Finite element model of implant and jawbone: **a** dimensions; and **b** load, boundary conditions and material properties

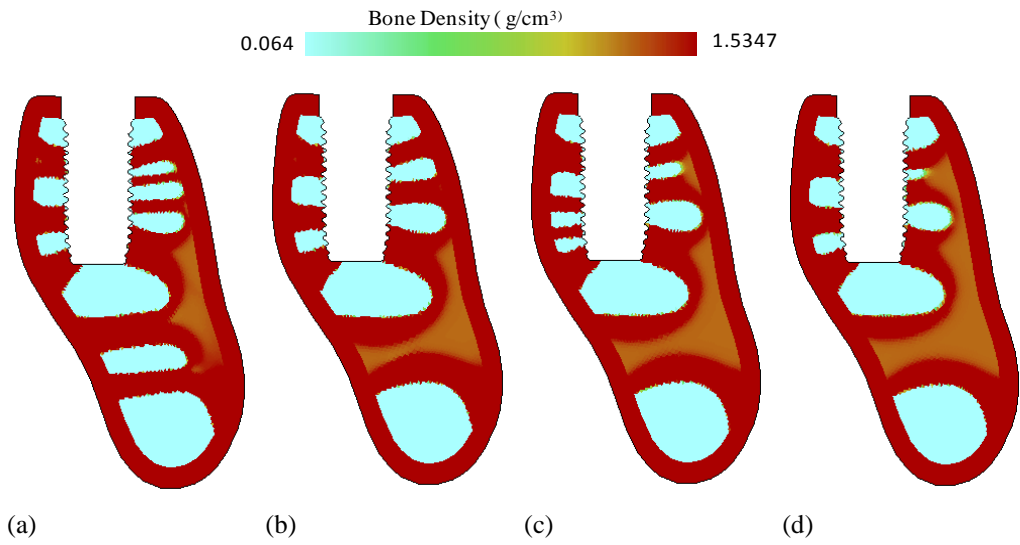


Fig. 5 Influence of 'lazy zone' effect on the density distribution of jawbone surrounding dental implant: **a** $s=0.1$; **b** $s=0.2$; **c** $s=0.3$; and **d** $s=0.4$

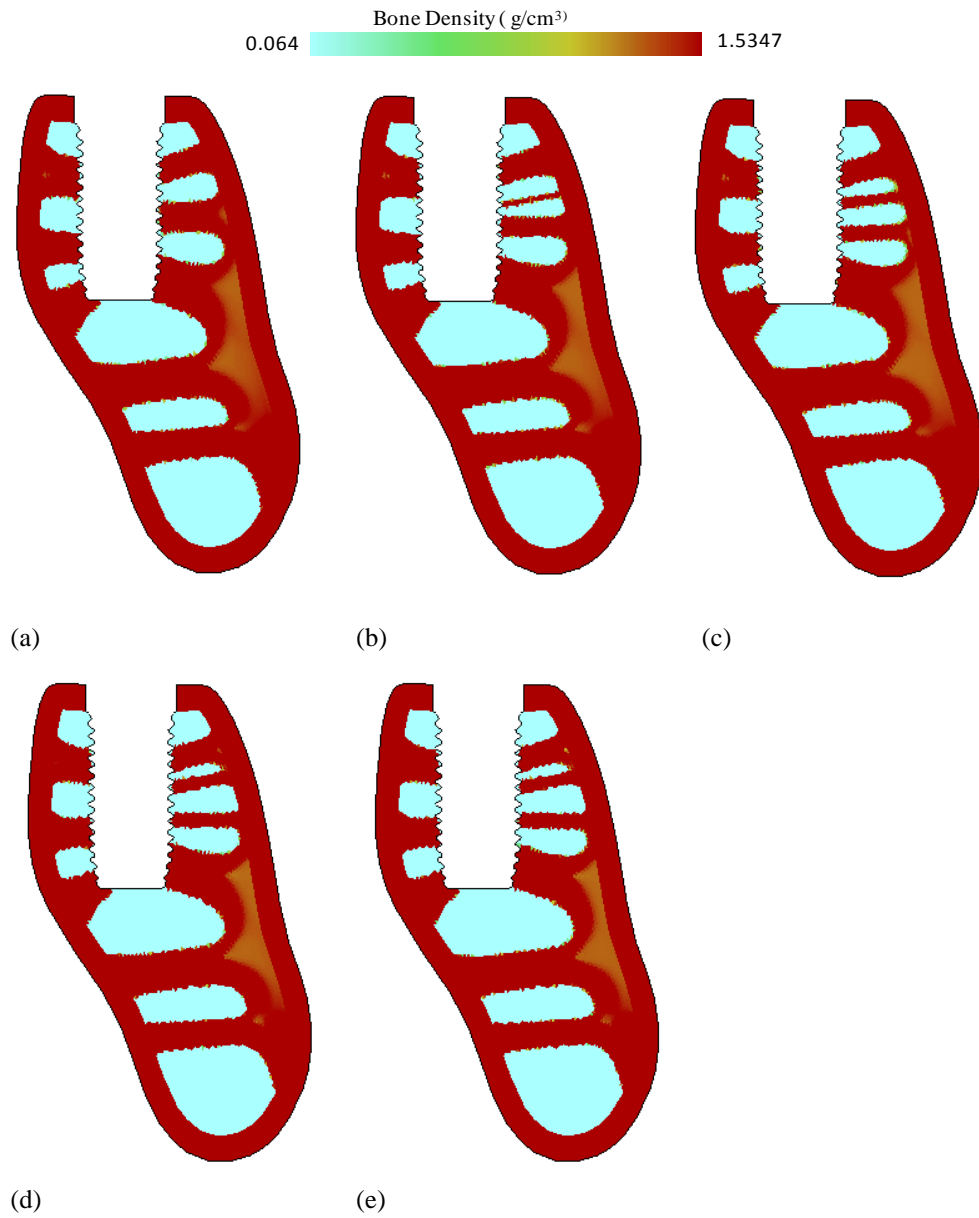
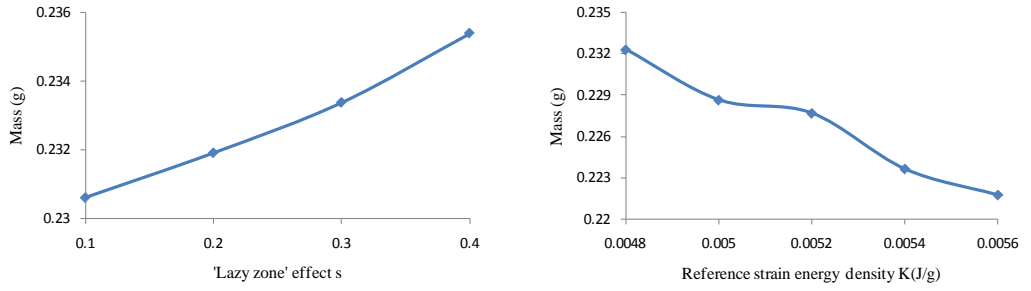
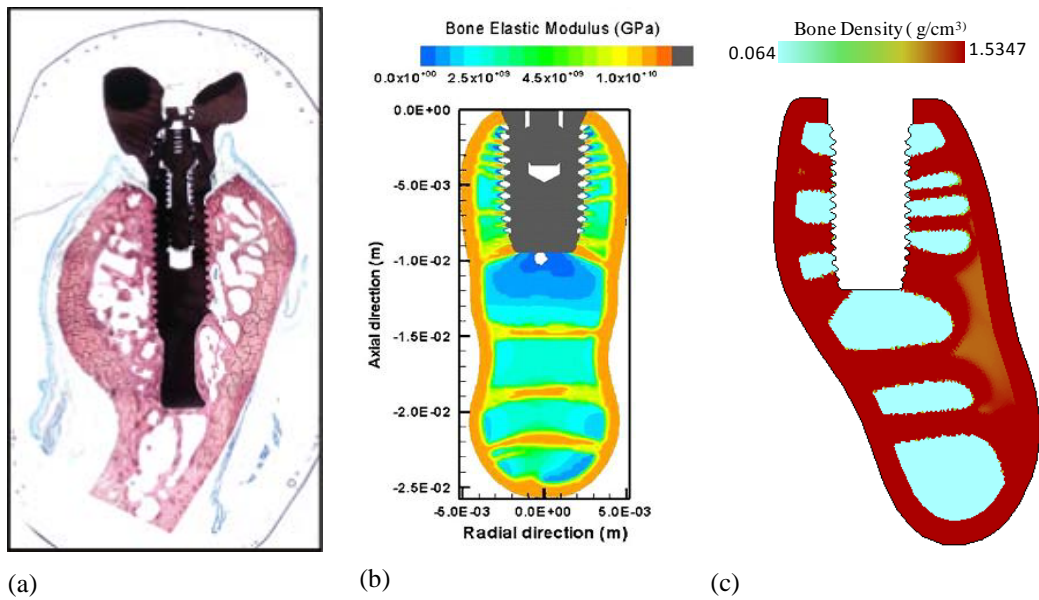


Fig. 6 Influence of reference SED value K on the density distribution of jawbone surrounding dental implant: **a** $K=0.0048$ J/g; **b** $K=0.005$ J/g; **c** $K=0.0052$ J/g; **d** $K=0.0054$ J/g; and **e** $K=0.0056$ J/g



(a) (b)
Fig. 7 Influence of two parameters on bone mass: **a** 'lazy zone' effect s ; and **b** reference value K



(a) (b) (c)
Fig. 8 Comparison of predicted result with clinical observations: **a** density distribution on baboons; **b** Chou et al.'s [33] prediction; and **c** predicted result with $K=0.0052$ J/g